Published in final edited form as:
Nature. ; 481(7382): 469–474. doi:10.1038/nature10737.

X-ray structures of LeuT in substrate-free outward-open and apo inward-open states

Harini Krishnamurthy[1] and **Eric Gouaux**[1,2]

[1]Vollum Institute, Oregon Health and Science University, 3181 SW Sam Jackson Park Road, Portland OR 97239 USA

[2]Howard Hughes Medical Institute, Oregon Health and Science University, 3181 SW Sam Jackson Park Road, Portland OR 97239 USA

Summary

Neurotransmitter sodium symporters are integral membrane proteins that remove chemical transmitters from the synapse and terminate neurotransmission mediated by serotonin, dopamine, noradrenaline, glycine and GABA. Crystal structures of the bacterial homolog, LeuT, in substrate-bound outward-occluded and competitive inhibitor-bound outward-facing states have advanced our mechanistic understanding of NSSs but have left fundamental questions unanswered. Here we report crystal structures of LeuT mutants in complexes with conformation-specific antibody fragments in the outward-open and inward-open states. In the absence of substrate but in the presence of sodium, the transporter is outward-open, illustrating how the binding of substrate closes the extracellular gate through local conformational changes: hinge-bending movements of the extracellular halves of TMs 1, 2, and 6, together with translation of EL4. The inward-open conformation, by contrast, involves large-scale conformational changes including a reorientation of TMs 1, 2, 5, 6, and 7, a dramatic hinge bending of TM1a and occlusion of the extracellular vestibule by EL4. These changes close the extracellular gate, open an intracellular vestibule, and largely disrupt the two sodium sites, thus providing a mechanism by which ions and substrate are released to the cytoplasm. The new structures establish a structural framework for the mechanism of neurotransmitter sodium symporters and their modulation by therapeutic and illicit substances.

Introduction

Chemical neurotransmission in the central nervous system is terminated through re-uptake of neurotransmitters from the synapse into surrounding neuronal and glial cells, a process first characterized by Hertting and Axelrod in 1961[1]. Transmitter uptake is mediated by neurotransmitter sodium symporters (NSS)[2,3], integral membrane proteins that exploit energetically favorable Na^+ electrochemical gradients for the thermodynamically uphill transport of neurotransmitters. Members of the NSS family include transporters for γ-amino butyric acid, glycine, norepinephrine, serotonin, and dopamine, chemical transmitters that

Correspondence and requests for materials should be addressed to E.G. (gouauxe@ohsu.edu). TEL: (503) 494-5535, FAX: (503) 494-1700.

Supplementary Information is linked to the online version of the paper at www.nature.com/nature.

Author Contributions

H.K. and E.G. contributed to all aspects of the project.

Competing financial interests

The authors declare no competing financial interests.

Atomic coordinates and structure factors have been deposited with the Protein Data Bank under codes 3TT1, 3TT3 and 3TU0 for the Y108F_LeuT^K–2B12 complex, the TSY_LeuT^K–6A10 complex and the TS_LeuT^K complex with alanine.

play fundamental roles in the function of the nervous system. Accordingly, dysfunction of these transporters is implicated in diseases such as depression[4,5], schizophrenia[4], epilepsy[6], and Parkinson's disease[4], and they are targets for therapeutic drugs including tricyclic antidepressants (TCAs) and selective serotonin re-uptake inhibitors (SSRIs) as well as addictive substances such as cocaine and amphetamines[7]. Understanding the substrate translocation mechanism of NSSs is central to the development of accurate models of substrate and drug complexes and to the discovery of new therapeutic agents.

The mechanism of NSS transport is generally described by the thermodynamically coupled binding of substrate and ion(s) to a central binding site that is alternately accessible to either side of the membrane[8,9] (SI Figure 1). Crystal structures of LeuT, a bacterial NSS homologue, elucidated the architecture of NSS proteins, demonstrated the existence of a substrate- and ion-bound occluded conformation, and illustrated how competitive and non-competitive inhibitors stabilize an outward-facing conformation[10–14]. LeuT is, at present, the best template for modeling the structure of NSSs and their complexes with therapeutic and illicit drugs. However, our understanding of mechanism and structure/function relationships in NSSs is incomplete due to the absence of LeuT structures in outward-open and inward-open states.

In the absence of structural knowledge of transporter intermediates, general mechanisms of transport have been proposed based on structures of other secondary transporters bearing the LeuT fold and crystallized in distinct conformational states[15–19]. However, low amino acid sequence identity compromises the extent to which this approach can generate a detailed and accurate mechanism for NSSs. Concomitantly, spectroscopic and computational methods have focused on characterization of conformational changes accompanying substrate and ion association/dissociation events in LeuT[20–23]. While these approaches have yielded new insights into localized movements, they have not revealed the three-dimensional, atomic-level details of conformational changes associated with substrate binding, isomerization of the transporter to the inward-open conformation, and release of substrate and sodium ion(s). Here, we present crystal structures of the outward-open and inward-open states of LeuT and thereby establish the structural basis for transport in the NSS family and provide accurate templates for modeling eukaryotic NSSs and their complexes with substrates, ions and drugs.

Stabilization of substrate-free and inward-open conformations

To stabilize substrate-free and inward-open states of LeuT, we mutated residues in TMs 3 and 8, helices comprising part of the 'scaffold' domain (TMs 3, 4, 8, and 9) and in TM6, one of the 'core' domain helices (TMs 1, 2, 6, and 7)[10,22,24] in the background of the wild-type-like K288A variant (LeuT^{K})[25] (SI Table 1, SI Figure 2). To further enhance crystallization behavior, we raised conformation-specific antibodies, exploiting fluorescence-detection size-exclusion chromatography (FSEC)[26] to select the antibodies and to demonstrate state-dependent binding. Well-diffracting crystals of substrate-free LeuT were obtained using the Tyr108 to Phe mutant in TM3 (Y108F_LeuT^{K})[25] and the 2B12 antibody fragment (Fab). Stabilization of LeuT in an inward-open conformation required weakening of the Na2 site by mutation of Thr354 to Val and Ser355 to Ala (TM8), as well as the cytoplasmic gate by changing Tyr268 to Ala (TM6; TSY_LeuT^{K})[23,27,28], together with the 6A10 Fab.

Sodium-bound state is outward-open

The substrate-free Y108F_LeuT^{K} structure (SI Table 2; SI Figure 3) adopts an outward-open conformation as a consequence of hinge-like movements in TMs 1b, 2a (residues 41–55), and 6a, relative to the outward-occluded state (Figure 1a–c, e). EL3 and TM11 are displaced by as much as 2.8 Å and 2.2 Å respectively, due to the movements of TM1b and

TM6a (Figure 1a). Strikingly, TMs 1b, 2a, and 6a pivot at Val23, Gly55, and Leu257, respectively, suggesting that when substrate no longer forges interactions between the core and scaffold domains, constraints on TM1b and TM6a are released, allowing them to move outward and the transporter to adopt an outward-open conformation. The Y108F_LeuT^K structure is similar to the previously reported Trp-bound LeuT structure[12] with a r.m.s.d value of 0.4 Å for all Cα atoms (SI Figure 4), supporting the general principle that inhibitors bind to conformational states populated by the wild-type transporter.

The 'thin' extracellular gate[19] of the outward-occluded state is ruptured in the Y108F_LeuT^K structure. Residues that bridge TM1b/TM6a to TM3/TM10 in the outward-occluded state have separated, opening a pathway to the extracellular solution (Figure 1d, e). Arg30 no longer forms a water-mediated salt bridge with Asp404 (TM10) and the side chain of Phe253 has rotated away from the binding site by a ~90° rotation about the χ1 dihedral angle, in agreement with molecular dynamics simulations[21,29]. The coordinated movement of Arg30 and Phe253 enables the retention of an important cation-π interaction between their respective guanidinium and phenyl groups. The phenyl ring of residue 253 now occupies the same position as the indole ring of Trp602 bound to the extracellular vestibule in the Trp-bound LeuT complex[12].

Prominent electron density peaks (4.0 σ) observed in the Na1 and Na2 sites together with ion-oxygen distances of ~ 2.4 Å[30] are consistent with sodium occupancy of these sites, although higher resolution diffraction data will be required to confirm their identity (Figure 2). Most importantly, the outward-open structure suggests that the presence of sodium ions keeps the intracellular thick gate[19] closed by bridging interactions between the intracellular halves of the core and scaffold domains. Even though the Na1 site is located close to the pivot points for TM1b and TM6a (Figure 2a), the concerted movement of the helices allows for retention of ion coordination geometry excepting the loss of the carboxylate oxygen from the absent substrate. Binding of Na^+ at this site may precede substrate binding, as also suggested by simulation studies[29], thereby stabilizing local conformations of TMs 1 and 6 and engaging the main chain carbonyl oxygen of Ala22 (TM1a) with side chain oxygens of Asn27 (TM1b) and Thr254 (TM6a). The Na2 site is located towards the intracellular region of TM1, stitching TM1a to TM8 through the main chain carbonyls of Gly20 and Val23 (Figure 2b). Thus, the Na^+ ions, through their interaction with TM1a, stabilize an intracellular-closed conformation, a finding supported by single molecule FRET studies[23].

Structure of the inward-open conformation

We hypothesized that weakening of the Na2 binding site by mutation of Thr354 and Ser355 to valine and alanine, respectively, and perturbation of the intracellular gate by mutation of Tyr268 to Ala[27], together yielding the TSY_LeuT^K variant, would shift the conformational equilibrium of LeuT towards the inward-open state (SI Discussion; SI Figures 2, 5, 8 and 9). We proceeded to crystallize the TSY_LeuT^K–6A10 Fab complex in the presence of lipids and solved the structure by molecular replacement at 3.2 Å resolution (SI Table 2, SI Figures 10, 11). Electron density for LeuT residues 1–10 was not observed and that for amino acids 11–24 was weak (mean B-factor of 158.0 Å^2 versus 121.2 Å^2 for the rest of LeuT). The Fab binds on the intracellular side of TSY_LeuT^K (SI Figure 11).

TSY_LeuT^K adopts an inward-open conformation as a consequence of large hinge-like movements within the core domain relative to the scaffold domain, and shifts in extracellular loops (Figures 3a–c). Perhaps the most striking change involves TM1a. Tilted by ~45° from its position in the closed state, it protrudes into the predicted location of the membrane. TM6b, in comparison, is rotated away from the central binding site by only 17°. In contrast to the uncoupled movements of TMs 1a and 6b, TMs 1b and 6a tilt by a similar

extent (24° and 21°, respectively) towards the scaffold domain, blocking the extracellular pathway. Because TM1 and TM6 do not move as a unit, we superimposed the inward-open and outward-occluded structures using only the scaffold domain, resulting in an r.m.s.d. in Cα positions of 3.0 Å. Helices buttressing TM1 and TM6, namely TM2, TM7, and TM5, also undergo substantial rearrangements but their extracellular and intracellular halves move to significantly different extents (Figure 3c). Thus, these helices bend, rather than tilt as rigid bodies, facilitated by either a glycine or proline residue located in their midsections. Movement of TM7 causes EL4 to dip down further into the extracellular vestibule, thus closing off the extracellular solvent pathway. To make room for TM6a, TM11 moves away from the center of the transporter, a direction opposite to that seen in the outward-open state (Figure 3b).

Access to the substrate binding site

In the inward-open LeuT structure, formation of a thick extracellular gate cuts off solvent access from the extracellular side while the thick intracellular gate opens, allowing access to the substrate binding site from the inside (Figures 3d–f). Consistent with cysteine accessibility studies on the serotonin (SERT)[22,31,32] and γ-amino butyric acid (GAT-1)[33] transporters, TM1a, TM5 and TM8 line the intracellular cavity. In particular, residues Leu14 and Ala19 of TM1a are solvent accessible, in line with the dramatic increase in reactivity observed for the corresponding residues in SERT in the inward-open conformation[22]. Accessibility and cross-linking studies also indicate that TM1b and TM6a move closer to TM3[34] and together with EL4 become inaccessible in the absence of sodium[35–38]. Consistent with its essential role in substrate transport[39], EL4 occludes the extracellular pathway by packing tightly against TM1b and TM7 on one side and TM3, TM8, and EL2 on the other side, making extensive contacts that include hydrophobic interactions and a hydrogen bond between Asp401 (TM10) and Ala319 (EL4).

The collapse of the extracellular vestibule in the inward-open state is central to our understanding of how therapeutic agents that include TCAs and SSRIs inhibit NSSs. Large, bulky molecules such as tryptophan[12], the cocaine analog 2β-carbomethoxy-3β-(4-iodophenyl)tropane[31], and SKF-8997A[40] arrest LeuT, SERT, and GAT-1, respectively, in the outward-facing conformation by blocking collapse of the extracellular vestibule, which in turn precludes opening of the intracellular gate. The inward-open LeuT structure now provides a new template for designing novel therapeutic agents that arrest NSS transporters in the inward-facing conformation. Ibogaine, shown to bind in the intracellular vestibule of SERT[41], is the only known inhibitor of this type.

The closure of the extracellular gate radically changes the nature of the proposed S2 substrate binding site that is hypothesized to be occupied by substrate in occluded and inward-facing conformational states[42,43]. Residues Ile111 and Leu400, stated to line the S2 site, are now deeply buried (SI Figure 12). Although we do see a small non-protein electron density feature near EL4, it is not likely a substrate molecule, not only because no substrates were included in the protein preparation, but also because the density cannot be well fit by leucine or a related amino acid. We suggest that the density is due to buffer, detergent or several water molecules.

Rupture and formation of gating interactions

The extracellular gate of the inward-open state is closed through interactions between residues of TM1b (Arg30) and TM10 (Asp404, Gly408, Thr409), EL4 (Ala319) and TM10 (Asp401) (Figure 4a) and TM6a (Asp240) and TM11 (Tyr471). The guanidinium group of Arg30, riding ‘on top’ of the aromatic ring of Phe253 (TM6a), makes multiple interactions with TM10 that include a direct salt-bridge with Asp404 and hydrogen bonds to Thr409 and

the carbonyl oxygen of Gly408. In GAT-1, conservative mutation to Lys of the residue equivalent to Arg30 severely compromises uptake activity[44], an outcome in accord with the manner in which interactions of Arg30 are modulated in the outward-open, outward-occluded, and inward-open states of LeuT (Fig. 4a,b).

In contrast to the extracellular gate, a network of interactions within the thick intracellular gate of outward-facing and outward-occluded states is disrupted (Fig. 4b,c). Ionic interactions linking the N-terminus and TM1a (Arg5, Trp8) to TM6b (Ser267, Tyr268) and TM8 (Gln361, Asp369) on the intracellular side no longer exist. The splaying apart of TM5, TM7, and TM1a also abrogates interactions between Lys196 and Thr10 and between Ser278 and Arg11. Consistent with the disruption of these interactions, mutation of residues homologous to Arg5 or Trp8[45], Tyr268[27,28], Asp369, Lys196, and Ser278[46,47] in eukaryotic transporters alters substrate uptake and shifts the conformational equilibrium of the transporter towards an inward-open state.

Perturbation of ion and substrate sites

The location of hinges for the conformational changes in TM1 and TM6 of the inward-open state has profound consequences for the substrate and sodium ion sites. The hinge for TM1a is located at Leu25, considerably ‘above’ the Na2 site, leading to separation of residues on TM1a and TM8 that define this site, thus demonstrating how the release of sodium from the Na2 site, the movement of TM1a and opening of the transporter to the cytoplasm are coupled (Figure 4c), a mechanism that has also been suggested for vSGLT[48]. There are two hinges in TM6, Ser256 for TM6a and Phe259 for TM6b, while TM1b also pivots at Leu25. Because these residues are all close to the substrate binding site but further away from the Na1 site (Figure 4e), there is minimal perturbation of the former (Figure 4d) but significant weakening of the latter (Figure 4e,f). Thus, while changes in TM1 and TM6 impact residues coordinating the α-amino group of leucine and cause small shifts in the side chains of Phe253 and Phe259, residues from TM3 and TM8 that engage the aliphatic moiety of the substrate maintain their positions. Consequently, an important portion of the substrate binding pocket is retained in the inward-open state, preserving the ability of the transporter to bind substrate under conditions of reversed substrate flux.

Structural principles of transporter mechanism

The pseudo 2-fold symmetric relationship of TMs 1–5 and 6–10 together with the organization of TMs 1, 2, 6 and 7 as a 4-helix bundle led to the rocking bundle mechanism of transport where the core moves as a unit about a rotation axis oriented approximately parallel to the membrane and intersecting the substrate binding site[22]. Detailed analysis of the inward-open state, however, indicates that only a portion of the core moves as a unit and there is not strict adherence to the pseudo 2-fold symmetry. The conformational transition from the outward-occluded to the inward-open state is brought about by multiple adjustments in individual TM helices, including the bending of TM2 and TM7 at conserved glycine residues and the independent movements of TMs 1a and 6b. Indeed, the core domains in the inward-open and outward-occluded states align with a r.m.s.d of 3.5 Å (Cα atoms), while the scaffold domains align with an r.m.s.d of 0.7 Å. If TM1a is excluded from consideration, however, the core domain helices superpose with a r.m.s.d of 0.83Å (Cα atoms), thus demonstrating that a portion of the core helices do reorient as a unit, undergoing a rotation of ~14° about an axis passing through Leu25 and Phe259 in the plane of the membrane (Figures 3a,c). The loops IL1 and EL4 are also related by the pseudo 2-fold symmetry axis, yet whereas EL4 undergoes large relative movements, the position of IL1 is constant.

The structural rearrangement of TM1a in the inward-open conformation of LeuT is different from that seen in Mhp1[15,18] in which TM1 moves as a rigid body (SI Fig 13)[22]. At present it is unclear whether the extent to which TM1a is seen to tilt away from its position in the occluded state reflects its true position in a native membrane environment. The fact that TM1a is neither involved in crystal contacts nor interacts with the Fab (SI Figure 11) diminishes the possibility that its position is a crystallization artefact. The weak density of TM1a suggests that it is highly flexible in the detergent/lipid micelles in which TSY_LeuT^{K} was crystallized. Indeed, the apparent mobility and large extent of movement of TM1a are in general agreement with findings of single molecule FRET studies and molecular dynamics simulations[23,49,50].

Coupling of binding sites and helix movements

The inward-open structure of LeuT suggests the manner by which changes in the sodium and substrate binding pockets are coupled to the larger structural changes that simultaneously open the intracellular side and close the extracellular side. The location of the TM1 hinge at Leu25 in the inward-open state, at a position extracellular to the substrate and sodium sites, is consistent with the observation that in the absence of Na^+ ions TM1a moves away from the scaffold domain and TM6b, not only initiating conformational changes that open an intracellular pathway, but also resulting in the disruption of the sodium ion sites. We propose that it is entropically unfavorable for TM1a to remain in an intracellular gate 'closed' conformation without the compensating enthalpic contribution from bound Na^+. We further suggest that the movement of TM1a initiates a cascade of structural rearrangements that result in closure of the extracellular gate as follows. A change in the position of TM1a requires movement of the intracellular region of TM5 (Figure 4g). Yet because TM5 lacks the hinge-like regions of TM1 and TM6, the entire helix tilts, 'pushing' TM7 and TM1b and closing the extracellular gate (Figure 3c). Similar structural adjustments involving TM2 and TM6a also occur ensuring that the intracellular gate cannot open without simultaneous closure of the extracellular gate.

Mechanism

Crystal structures of LeuT captured in three distinct conformational states show how both local conformational changes and rigid body movements of groups of helices are associated with the transport mechanism (Figure 5). Opening and closure of the extracellular and intracellular gates exploit hinge-like bending of helices at pivot points within short non-helical regions halfway across the bilayer, together with the rigid body rotation of helical bundles, movements of extracellular loops and flexing of numerous transmembrane helices (SI Movie). General principles emerging from these studies are that local hinge-like movements of transmembrane helices are coupled to the formation and disruption of substrate and sodium binding sites which are translated through nearly rigid body movements of groups of helices and loops into opening and closing of the 'thick' extracellular and intracellular gates. Most importantly, the relative locations of substrate/ion binding sites and hinge pivots define the extent to which hinge motions perturb the sites. More broadly, these structures demonstrate how the overall conformation and shape of LeuT changes during the transport cycle, thereby providing a general mechanistic framework to understand how substrates, ions, mutations and drugs modulate the conformational equilibria and transport activity of LeuT and related NSS proteins.

Methods Summary

LeuT mutants were expressed as previously described[10], monoclonal antibodies and Fabs were generated by standard methods, and x-ray crystal structures of the Fab complexes were

solved by molecular replacement. Final models were obtained by an iterative process of manual model building and refinement against X-ray diffraction data. The functional properties of LeuT mutants were examined using scintillation proximity binding assays and uptake or exchange assays with LeuT reconstituted into proteoliposomes.

Methods

Purification of LeuT mutants

The site-directed mutants Y108F_LeuT^K, TS_LeuT^K, and TSY_LeuT^K were produced by the polymerase chain reaction and subcloned into a pET16b plasmid containing a thrombin-cleavage site and a C-terminal octa-histidine tag. All mutants were verified by DNA sequencing. The resulting proteins were expressed and purified as previously described[10,25] with the following modifications. To obtain leucine-free transporter, buffers for purification did not contain sodium salts and membranes were washed three times in sodium-free buffer to ensure that no endogenously-bound leucine was carried along. LeuT mutants were solubilized with *n*-dodecyl-β-D-maltopyranoside ($C_{12}M$) and purified by Ni-affinity chromatography. Protein for functional and biochemical assays was further purified by gel filtration in buffer containing $C_{12}M$.

Production and purification of monoclonal antibodies and Fab fragments

Mouse monoclonal antibodies (mAb) against Y108F_LeuT^K and TSY_LeuT^K were raised by standard methods using corresponding purified protein in detergent as antigen. Antibodies recognizing a conformational epitope in Y108F_LeuT^K were selected using FSEC[26] and Western blot analysis, resulting in the identification of the 2B12 mAb. Antibodies specific to the inward-facing mutant TSY_LeuT^K were selected based on their relative affinities for TSY_LeuT^K and wild-type LeuT as determined by FSEC. From these screens we isolated the 6A10 mAb. All FSEC analysis relied on C-terminal GFP-fusions of the LeuT variants. Antibodies were purified from hybridoma supernatants using a SP sepharose cation-exchange column. Fab fragments were generated by papain digestion at 37 °C in 50 mM sodium phosphate pH 7.2, 1 mM EDTA and a papain to mAb ratio of 1:20 w/w (2B12) or 1:100 w/w (6A10). Cysteine at 10 mM final concentration was added to the digestion reaction for 6A10. Digestion of 2B12 was stopped with 30 mM iodoacetamide after 4 hours, while digestion of 6A10 was quenched by transferring the reaction to 4°C after 2 hours. Fab fragments were purified on a Protein A column, followed by ion-exchange chromatography. DNA encoding the light and heavy chains of 2B12 (IgG2a, κ) and 6A10 (IgG1, κ) Fab fragments were cloned and sequenced from hybridoma cells using 5′-RACE.

Purification of Fab complexes for crystallization

The His-tag of LeuT destined for crystallization was cleaved by thrombin. Transporter was then mixed with excess Fab and the complex was subjected to gel-filtration in *n*-octyl-β-D-thioglucopyranoside (C_8SG) containing buffer. The buffer consisted of 20 mM Tris, pH 8.0, 50 mM (TSY_LeuT^K-Fab) or 100 mM (Y108F_LeuT^K-Fab) KCl, and 12 mM (TSY_LeuT^K-Fab) or 15 mM (Y108F_LeuT^K-Fab) C_8SG. For crystallization of TSY_LeuT^K-Fab complex, the protein was then supplemented with a 5-fold molar excess of 1,2-dimyristoyl-*sn*-glycero-3-phosphoethanolamine (DMPE) and incubated at 4°C for 1 hour before removing insoluble lipids by centrifugation. A 55 mM DMPE stock was prepared in 20% DMSO and 80% gel filtration buffer. Protein was concentrated to 3.0–3.2 mg/ml (Y108F_LeuT^K-Fab) or 4.5–5 mg/ml (TSY_LeuT^K-Fab) for crystallization.

Crystallization

Crystallization was carried out by vapor diffusion in hanging drops at 20 °C. Y108F_LeuT^K-Fab crystals were grown in 40 mM Tris pH 7.5, 23–26% PEG 550 monomethyl ether, and 50–100 mM NaCl and cryo-protected in 35% PEG 550 monomethyl ether. Crystals were allowed to sit in the final cryo-solution for 4–5 hours before flash freezing in liquid nitrogen.

Different crystal forms were obtained for the TSY_LeuT^K-Fab complex in similar crystallization conditions with the best crystals belonging to space group $C222_1$. These crystals were grown in 100 mM HEPES pH 7.6, 0.1 M $Mg(NO_3)_2$, 12–14% PEG 1500, and 1.5% w/v trimethylamine *N*-oxide dehydrate in protein to precipitant ratio of 1:2. TSY_LeuT^K-Fab crystals were cryo-protected with 15 % PEG 1500 and 20% glycerol before flash-freezing.

Crystals of alanine-bound TS_LeuT^K were obtained from protein purified in 20 mM Tris pH 8.0, 100 mM L-Ala, 200 mM NaCl, and 40 mM β-OG (*n*-octyl-β-D-glucoside). Purification and crystallization were carried out as described for wild-type LeuT[10].

Data collection and structure determination

The Y108F_LeuT^K-Fab complex. X-ray diffraction data sets for the Y108F_LeuT^K-Fab crystals were indexed, integrated and scaled using HKL2000 and CCP4 suite of computer programs[51,52]. The crystals diffract to ~3.1 Å resolution, belong to the space group $P2_12_12_1$ and harbor 2 Y108F_LeuT^K-Fab complexes per asymmetric unit giving a Matthews coefficient[53] of 3.9 Å^3/Da. The structure was determined by molecular replacement using the program PHASER[54]. The search probes were the tryptophan-bound LeuT structure (pdbcode: 3F3A) and a Fab homology model built using SWISS-MODEL[55]. The model was built using COOT[56] into $2F_o$-F_c maps, cross-validated using simulated annealing composite omit maps and refined with PHENIX[57] using non crystallographic symmetry, individual atomic displacement parameters and translation/libration/screw (TLS)[58] subdomains. Six TLS groups composed of 2 LeuT molecules, 2 Fab constant domains and 2 Fab variable domains were defined. This iterative model building and refinement procedure yielded a structure with good crystallographic and stereochemical statistics. Regions of weak or no electron density were excluded from the model such that the final structure consists of LeuT residues 5–129 and 135–507, Fab light chain residues 1–215, and Fab heavy chain residues 1–135, 143–219.

The TSY_LeuT^K-Fab complex—The crystals diffract to ~3.2 Å resolution and belong to the space group $C222_1$. There is one complex in the asymmetric unit resulting in a Matthews coefficient of 3.4 Å^3/Da. Initial phases were derived from a molecular replacement solution using PHASER[54] in which a partial structure of leucine-bound LeuT (pdbcode: 2A65) and a high resolution IgG1 Fab structure (pdbcode: 1Q9Q) were used as search probes. The partial LeuT search probe was obtained by deleting TMs 1, 6, and 12 from the 2A65 structure. Electron density maps calculated using the "Prime and Switch" method[59] clearly showed the LeuT regions where there were deviations from the 2A65 structure. This initial molecular replacement solution was used as a starting point for automated building using Phenix. Further changes were made to the LeuT portion using COOT[56]. At this stage, electron density for the Fab portion was poor, making it difficult for manual building. A homology model built using PDB 1EJO for the light chain and PDB 2Z4Q for the heavy chain by PHYRE[60] resulted in a substantial decrease in the crystallographic R-factors, yielding R_{work} and R_{free} of 0.33 and 0.36, respectively. This model and a $2F_o$-F_c map calculated with exclusion of the test set of reflections (R_{free} set) were then submitted to a crystallographic refinement server developed by Haddadian et al. (http://godzilla.uchicago.edu). The

resulting model had improved stereochemistry and R_{work} and R_{free} of 0.29 and 0.32, respectively.

Further improvements to the model were made until the R_{work} /R_{free} converged to 0.26/0.30 and structure quality assessed using Molprobity[61] was satisfactory. Throughout the model building procedure, bias-minimized 'Prime and Switch' maps[59] and simulated annealing composite omit maps were used. Individual isotropic B factors and TLS parameters were refined using 11 TLS groups identified using Phenix[57]: 3 LeuT domains comprised of residues 11–184, 185–254, and 255–511, 4 Fab heavy chain domains involving residues 1–83, 84–140, 141–180, and 181–219, together with residues 1–94, 95–131, 132–177, and 178–215 forming the 4 Fab light chain domains. The final model consists of LeuT residues 11–511, Fab light chain residues 1–216, Fab heavy chain residues 1–102, 104–219, and several detergent molecules.

The changes in helix and domain orientation were analyzed using the program Interhlx (K. Yap, University of Toronto) and DynDom, respectively, and molecular figures were prepared using PyMOL.

Saturation binding assays

Dissociation constants of LeuT mutants for leucine were determined by scintillation proximity assays as described earlier[25] at a protein concentration of 1 μM in 20 mM Tris-MES pH 7.0, 200 mM NaCl, and 1mM $C_{12}M$. Non-specific binding was measured in duplicate using 1 mM L-Leucine as cold-competitor and total binding was measured in triplicate. Data were fit with GraphPad Prism.

Transport time course

LeuT mutants were reconstituted into liposomes as previously described[25] at a protein to lipid ratio of 1:100 and loaded with either Buffer 1 (20 mM Tris-MES pH 6.0 and 500 mM KCl) for uptake or Buffer 2 (20 mM Tris-MES pH 6.0, 500 mM NaCl, and 10 mM L-Leucine) for exchange. Transport was initiated at 27 °C by diluting proteoliposomes to 10 μg/ml into external buffer (20 mM Tris-MES pH 6.0, 500 mM NaCl) containing either 200 nM (for Y108F_LeuT^K) or 400 nM (for TS_LeuT^K and TSY_LeuT^K) or 10nM[^{3}H]-Leucine for LeuTK. Uptake or exchange was followed by quenching 100 μl samples of the reaction mixture in 1.8 ml of ice-cold Buffer 1 for uptake or Buffer 2 for exchange. Background counts were measured with control reactions performed in the absence of sodium. Reactions were measured in replicates of 3–5 and analyzed using GraphPad Prism.

Fluorescence-detection size-exclusion chromatography

FSEC experiments[26] were carried out using a Superose 6 10/300 column with the mobile phase consisting of 20 mM Tris, pH 8.0, 1mM $C_{12}M$, and either 200–400 mM NaCl and 10 mM leucine or 200 mM KCl for analyses of LeuT in substrate-bound and apo states, respectively. Fab-LeuT complexes were prepared by mixing LeuT and Fab in a molar ratio of 1:2. Elution was followed using tryptophan fluorescence with excitation and emission wavelengths at 280 nm and 335 nm, respectively.

Supplementary Material

Refer to Web version on PubMed Central for supplementary material.

Acknowledgments

We thank D. Cawley for monoclonal antibody production, L. Vaskalis for help with illustrations and the staff at the Advanced Photon Source beamline 24-ID-E and at the Advanced Light Source beamline 5.0.2 for their assistance with X-ray data collection and processing. We are grateful to E. Haddadian, T. Sosnick and K. Freed for assistance in refining the backbone torsional and side chain angles using their unpublished TOP algorithm. We thank all Gouaux laboratory members, especially C. Piscitelli and S. K. Singh, for discussions and helpful suggestions throughout the project. This work was supported by the NIH. E.G. is an investigator with the Howard Hughes Medical Institute.

References

1. Hertting G, Axelrod J. Fate of tritiated noradrenaline at the sympathetic nerve-endings. Nature. 1961; 192:172–173. [PubMed: 13906919]
2. Nelson N. The family of Na+/Cl- neurotransmitter transporters. J Neurochem. 1998; 71:1785–1803. [PubMed: 9798903]
3. Saier MHJ. A functional-phylogenetic classification system for transmembrane solute transporters. Microbiol Mol Biol Rev. 2000; 64:354–411. [PubMed: 10839820]
4. Hahn MK, Blakely RD. Monoamine transporter gene structure and polymorphisms in relation to psychiatric and other complex disorders. Pharmacogenomics J. 2002; 2:217–235. [PubMed: 12196911]
5. Klimek V, et al. Reduced levels of norepinephrine transporters in the locus coeruleus in major depression. J Neurosci. 1997; 17:8451–8458. [PubMed: 9334417]
6. Richerson GB, Wu Y. Role of the GABA transporter in epilepsy. Adv Exp Med Biol. 2004; 548:76–91. [PubMed: 15250587]
7. Amara SG, Sonders MS. Neurotransmitter transporters as molecular targets for addictive drugs. Drug Alcohol Depend. 1998; 51:87–96. [PubMed: 9716932]
8. Mitchell P. A general theory of membrane transport from studies of bacteria. Nature. 1957; 180:134–136. [PubMed: 13451664]
9. Jardetzky O. Simple allosteric model for membrane pumps. Nature. 1966; 211:969–970. [PubMed: 5968307]
10. Yamashita A, Singh SK, Kawate T, Jin Y, Gouaux E. Crystal structure of a bacterial homologue of Na+/Cl- - dependent neurotransmitter transporters. Nature. 2005; 437:215–223. [PubMed: 16041361]
11. Singh S, Yamashita A, Gouaux E. Antidepressant binding site in a bacterial homologue of neurotransmitter transporters. Nature. 2007; 448:952–956. [PubMed: 17687333]
12. Singh SK, Piscitelli CL, Yamashita A, Gouaux E. A competitive inhibitor traps LeuT in an open-to-out conformation. Science. 2008; 322:1655–1661. [PubMed: 19074341]
13. Zhou Z, et al. LeuT-desipramine structure reveals how antidepressants block neurotransmitter uptake. Science. 2007; 317:1390–1393. [PubMed: 17690258]
14. Zhou Z, et al. Antidepressant specificity of serotonin transporter suggested by three LeuT-SSRI structures. Nature Struct Mol Biol. 2009; 16:652–657. [PubMed: 19430461]
15. Weyand S, et al. Structure and molecular mechanism of a nucleobase-cation-symport-1 family transporter. Science. 2008; 322:709–713. [PubMed: 18927357]
16. Faham S, et al. The crystal structure of a sodium galactose transporter reveals mechanistic insights into Na+/sugar symport. Science. 2008; 321:810–814. [PubMed: 18599740]
17. Shaffer PL, Goehring A, Shankaranarayanan A, Gouaux E. Structure and mechanism of a Na+-independent amino acid transporter. Science. 2009; 325:1010–1014. [PubMed: 19608859]
18. Shimamura T, et al. Molecular basis of alternating access membrane transport by the sodium-hydantoin transporter Mhp1. Science. 2010; 328:470–473. [PubMed: 20413494]
19. Krishnamurthy H, Piscitelli CL, Gouaux E. Unlocking the molecular secrets of sodium-coupled transporters. Nature. 2009; 459:347–355. [PubMed: 19458710]
20. Shaikh SA, Tajkhorshid E. Modeling and dynamics of the inward-facing state of a Na+/Cl-dependent neurotransmitter transporter homologue. PLoS Comput Biol. 2010; 6:e1000905. [PubMed: 20865057]

21. Claxton DP, et al. Ion/substrate-dependent conformational dynamics of a bacterial homolog of neurotransmitter:sodium symporters. Nat Struct Mol Biol. 2010; 17:822–829. [PubMed: 20562855]
22. Forrest LR, et al. Mechanism for alternating access in neurotransmitter transporters. Proc Natl Acad Sci USA. 2008; 105:10338–10343. [PubMed: 18647834]
23. Zhao Y, et al. Single-molecule dynamics of gating in a neurotransmitter transporter homologue. Nature. 2010; 465:188–193. [PubMed: 20463731]
24. Boudker O, Verdon G. Structural perspectives on secondary active transporters. Trends Pharmacol Sci. 2010; 31:418–426. [PubMed: 20655602]
25. Piscitelli CL, Krishnamurthy H, Gouaux E. Neurotransmitter/sodium symporter orthologue LeuT has a single high-affinity substrate site. Nature. 2010; 468:1129–1132. [PubMed: 21179170]
26. Kawate T, Gouaux E. Fluorescence-detection size-exclusion chromatography for precrystallization screening of integral membrane proteins. Structure. 2006; 14:673–681. [PubMed: 16615909]
27. Kniazeff J, et al. An intracellular interaction network regulates conformational transitions in the dopamine transporter. J Biol Chem. 2008; 283:17691–17701. [PubMed: 18426798]
28. Loland CJ, Norregaard L, Litman T, Gether U. Generation of an activating Zn(2+) switch in the dopamine transporter: Mutation of an intracellular tyrosine constitutively alters the conformational equilibrium of the transport cycle. Proc Natl Acad Sci USA. 2002; 99:1683–1688. [PubMed: 11818545]
29. Celik L, Schiott B, Tajkhorshid E. Substrate binding and formation of an occluded state in the leucine transporter. Biophys J. 2008; 94:1600–1612. [PubMed: 18024499]
30. Harding MM. Small revisions to predicted distances around metal sites in proteins. Acta Crystallogr D Biol Crystallogr. 2006; 62:678–682. [PubMed: 16699196]
31. Zhang YW, Rudnick G. The cytoplasmic substrate permeation pathway of serotonin transporter. J Biol Chem. 2006; 281:36213–36220. [PubMed: 17008313]
32. Rudnick G. The cytoplasmic permeation pathway of neurotransmitter transporters. Biochemistry. 2011; 50:7462–7475. [PubMed: 21774491]
33. Ben-Yona A, Kanner BI. Transmembrane domain 8 of the γ-aminobutyric acid transporter GAT-1 lines a cytoplasmic accessibility pathway into its binding pocket. J Biol Chem. 2009; 284:9727–9732. [PubMed: 19201752]
34. Tao Z, Zhang YW, Agyiri A, Rudnick G. Ligand effects on cross-linking support a conformational mechanism for serotonin transport. J Biol Chem. 2009; 284:33807–33814. [PubMed: 19837674]
35. Rosenberg A, Kanner BI. The substrates of the gamma-aminobutyric acid transporter GAT-1 induce structural rearrangements around the interface of transmembrane domains 1 and 6. J Biol Chem. 2008; 283:14376–14383. [PubMed: 18381286]
36. Henry LK, Adkins EM, Han Q, Blakely RD. Serotonin and cocaine-sensitive inactivation of human serotonin transporters by methanethiosulfonates targeted to transmembrane domain I. J Biol Chem. 2003; 278:37052–37063. [PubMed: 12869570]
37. Zomot E, Kanner BI. The interaction of the gamma-aminobutyric acid transporter GAT-1 with the neurotransmitter is selectively impaired by sulfhydryl modification of a conformationally sensitive cysteine residue engineered into extracellular loop IV. J Biol Chem. 2003; 278:42950–42958. [PubMed: 12925537]
38. Mitchell SM, Lee E, Garcia ML, Stephan MM. Structure and function of extracellular loop 4 of the serotonin transporter as revealed by cysteine-scanning mutagenesis. J Biol Chem. 2004; 279:24089–24099. [PubMed: 15140876]
39. Smicun Y, Campbell SD, Chen MA, Gu H, Rudnick G. The role of external loop regions in serotonin transport. Loop scanning mutagenesis of the serotonin transporter external domain. J Biol Chem. 1999; 274:36058–36064. [PubMed: 10593887]
40. Hirayama BA, Diez-Sampedro A, Wright EM. Common mechanisms of inhibition for the Na+/glucose (hSGLT1) and Na+/Cl-/GABA (hGAT1) cotransporters. Br J Pharmacol. 2001; 134:484–495. [PubMed: 11588102]
41. Jacobs MT, Zhang YW, Campbell SD, Rudnick G. Ibogaine, a noncompetitive inhibitor of serotonin transport, acts by stabilizing the cytoplasm-facing state of the transporter. J Biol Chem. 2007; 282:29441–29447. [PubMed: 17698848]

42. Shi L, Quick M, Zhao Y, Weinstein H, Javitch JA. The mechanism of a neurotransmitter:sodium symporter-inward release of Na+ and substrate is triggered by a substrate in a second binding site. Mol Cell. 2008; 30:667–677. [PubMed: 18570870]
43. Zhao Y, et al. Substrate-modulated gating dynamics in a Na(+)-coupled neurotransmitter transporter homologue. Nature. 2011; 474:109–113. [PubMed: 21516104]
44. Pantanowitz S, Bendahan A, Kanner BI. Only one of the charged amino acids located in the transmembrane α-helices of the γ-aminobutyric acid transporter (Subtype A) is essential for its activity. J Biol Chem. 1993; 268:3222–3225. [PubMed: 8428999]
45. Bennett ER, Su H, Kanner BI. Mutation of arginine 44 of GAT-1, a (Na(+) + Cl(−))-coupled gamma-aminobutyric acid transporter from rat brain, impairs net flux but not exchange. J Biol Chem. 2000; 275:34106–34113. [PubMed: 10926932]
46. Loland CJ, Granas C, Javitch JA, Gether U. Identification of intracellular residues in the dopamine transporter critical for regulation of transporter conformation and cocaine binding. J Biol Chem. 2004; 279:3228–3238. [PubMed: 14597628]
47. Chen N, Rickey J, Berfield JL, Reith ME. Aspartate 345 of the dopamine transporter is critical for conformational changes in substrate translocation and cocaine binding. J Biol Chem. 2004; 279:5508–5519. [PubMed: 14660644]
48. Watanabe A, et al. The mechanism of sodium and substrate release from the binding pocket of vSGLT. Nature. 2010; 468:988–991. [PubMed: 21131949]
49. Quick M, et al. State-dependent conformations of the translocation pathway in the tyrosine transporter Tyt1, a novel neurotransmitter:sodium symporter from Fusobacterium nucleatum. J Biol Chem. 2006; 281:26444–26454. [PubMed: 16798738]
50. Shi L, Weinstein H. Conformational rearrangements to the intracellular open states of the LeuT and ApcT transporters are modulated by common mechanisms. Biophys J. 2010; 99:L103–105. [PubMed: 21156121]
51. Otwinowski Z, Minor W. Processing of X-ray diffraction data collected in oscillation mode. Meth Enzymol. 1997; 276:307–326.
52. CCP4 Project, N. The *CCP4* suite: programs for protein crystallography. Acta Crystallogr. 1994; D50:760–763.
53. Matthews BW. Solvent content of protein crystals. J Mol Biol. 1968; 33:491–497. [PubMed: 5700707]
54. McCoy AJ. Solving structures of protein complexes by molecular replacement with Phaser. Acta Crystallogr D. 2007; 63:32–41. [PubMed: 17164524]
55. Kopp J, Schwede T. The SWISS-MODEL Repository: new features and functionalities. Nucleic Acids Res. 2006; 34:D315–D318. [PubMed: 16381875]
56. Emsley P, Cowtan K. Coot: model-building tools for molecular graphics. Acta Crystallogr D. 2004; 60:2126–2132. [PubMed: 15572765]
57. Adams PD, et al. PHENIX: building new software for automated crystallographic structure determination. Acta Crystallogr D. 2002; 58:1948–1954. [PubMed: 12393927]
58. Painter J, Merritt EA. Optimal description of a protein structure in terms of multiple groups undergoing TLS motion. Acta Crystallogr D. 2006; 62:439–450. [PubMed: 16552146]
59. Terwilliger TC. Using prime-and-switch phasing to reduce model bias in molecular replacement. Acta Crystallogr D Biol Crystallogr. 2004; 60:2144–2149. [PubMed: 15572767]
60. Kelley LA, Sternberg MJ. Protein structure prediction on the Web: a case study using the Phyre server. Nat Protoc. 2009; 4:363–371. [PubMed: 19247286]
61. Chen VB, et al. MolProbity: all-atom structure validation for macromolecular crystallography. Acta Crystallogr D Biol Crystallogr. 66:12–21. [PubMed: 20057044]

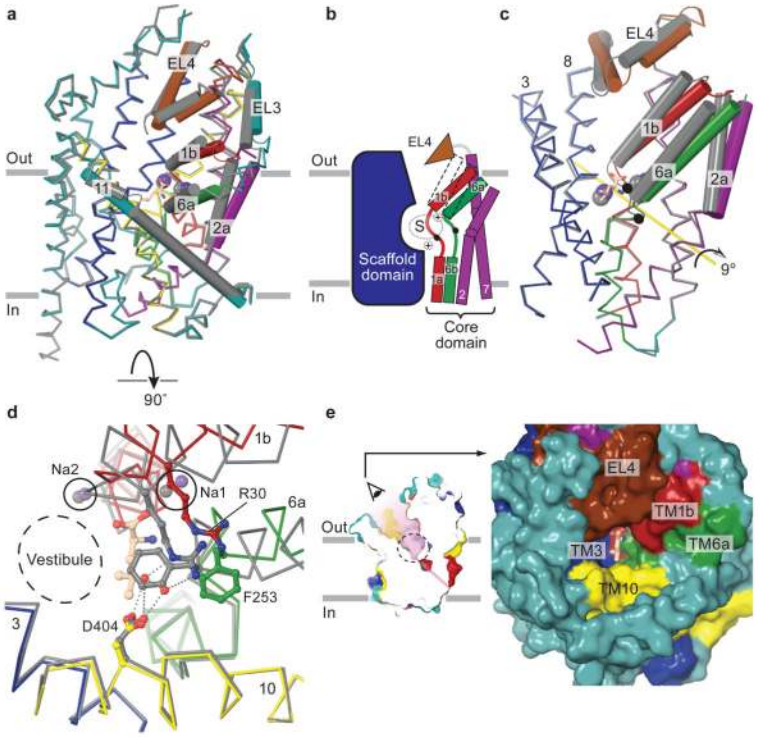

Figure 1. Substrate-free, Na^+-bound state is outward-open

a, Superposition of the outward-open and leucine-bound outward-occluded conformations. Outward-open structure is colored with Na^+ ions as purple spheres. The outward-occluded structure with Na^+ ions (spheres) is grey and leucine in stick representation. **b,** Schematic of scaffold and core domains, EL4, the pivot points of hinge movements in TMs 1 and 6 (solid black circles) and the substrate (S) and sodium sites (+). **c,** Superposition, as in panel **a**, illustrating that a ~9° rotation about an axis passing through the middle of the core domain (yellow arrow) describes the conformational change associated with opening to the outside. Pivot points are shown as in panel **b. d,** Rupture of extracellular gate interactions (grey dashed lines) in the outward-open structure. Two water molecules that bridge Arg 30 and Asp 404 in the outward-occluded state are shown as red spheres. **e,** Surface representation of the outward-open structure with the zig-zag pink line indicating a closed intracellular pathway. Leucine, where shown, is from the outward-occluded Leu-bound structure.

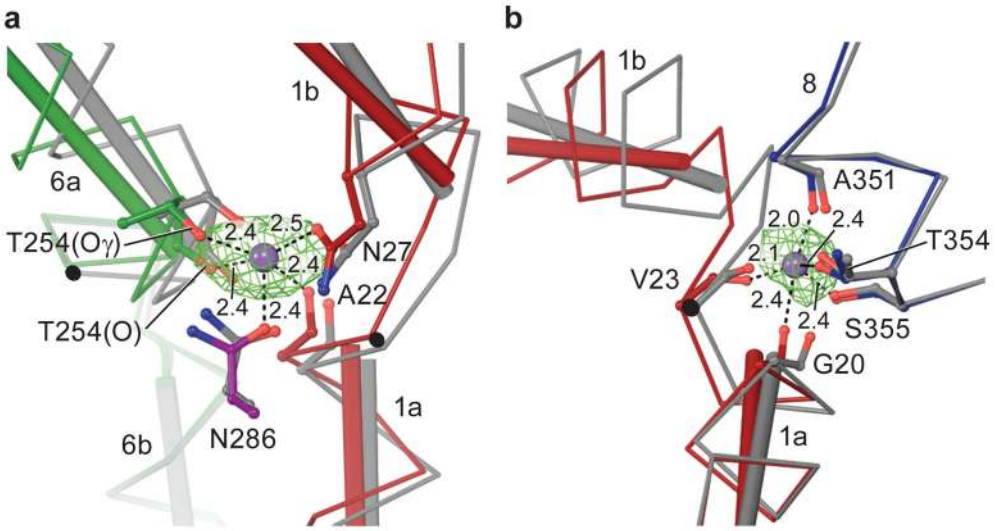

Figure 2. Sodium sites in outward-open state

a, The Na1 site showing positions of the coordinating residues within the framework of global changes in the outward-open structure. **b,** The Na2 site. F_o - F_c omit density is contoured at 4 σ and represented as green mesh. Coloring scheme and representations are the same as in Fig. 1. Dashed lines indicate interactions between sodium ions and coordinating atoms with distances in Å, solid black circles are approximate pivot points for hinge movement of helices and red and green cylinders define the TM1 and 6 helix axes, respectively.

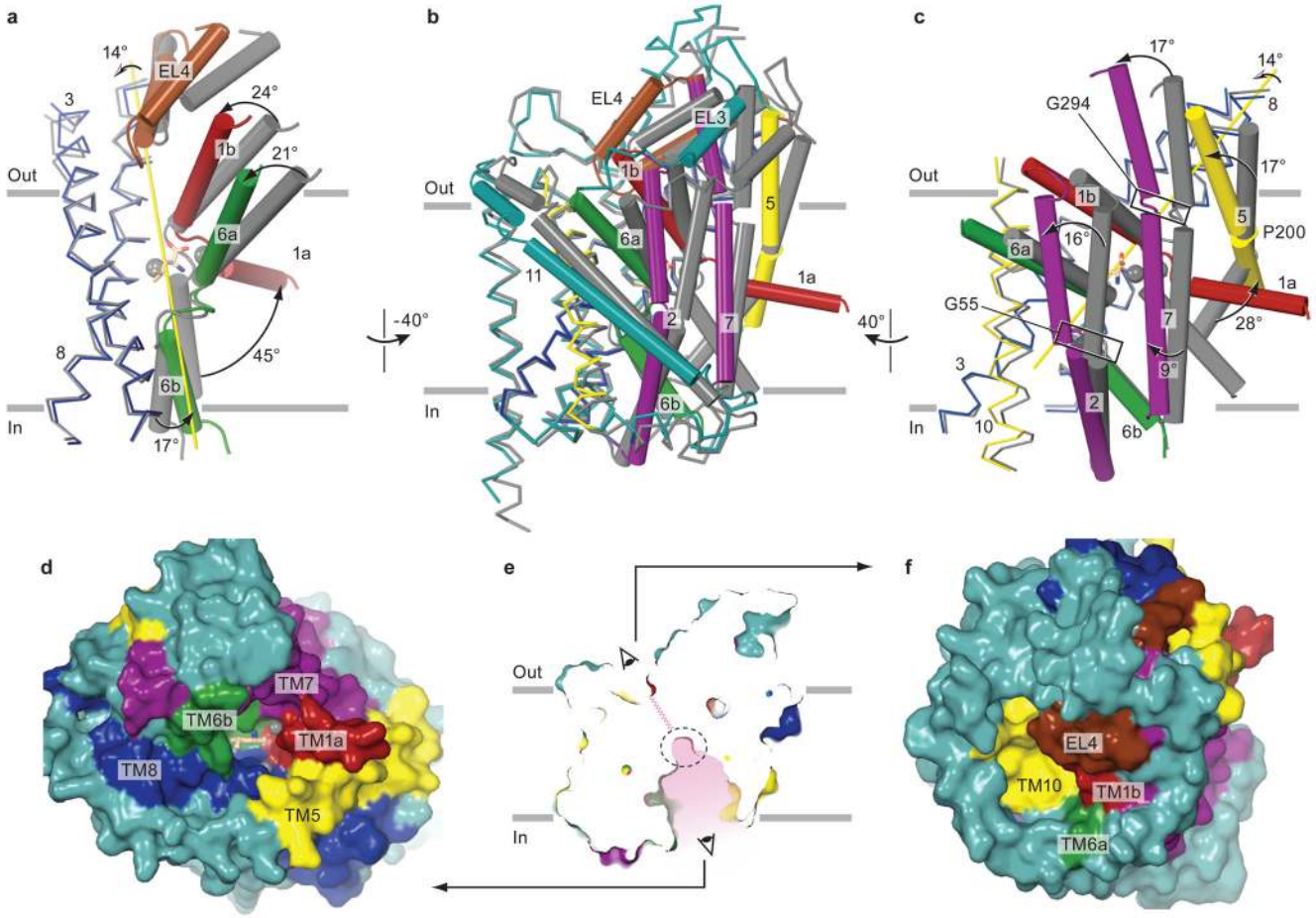

Figure 3. Inward-open conformation

a–c, Superposition of inward-open and outward-occluded state structures using the scaffold domain. The overall changes shown in **b** are divided in two parts, **a** and **c,** for clarity. The extent of rotation for the key TMs between the outward-occluded and inward-open conformations are indicated in **a** and **c**. The axis of rotation of core domain with the exclusion of TM1a is depicted in yellow. **d,** Surface representation of the inward-open structure looking 'up' into the binding site from intracellular side as indicated in **e. f,** Surface representation of the inward-open structure showing the elements forming the extracellular thick gate. Color coding and representations are as in Fig. 1. Leucine and sodium, where shown, are from the outward-occluded Leu-bound structure.

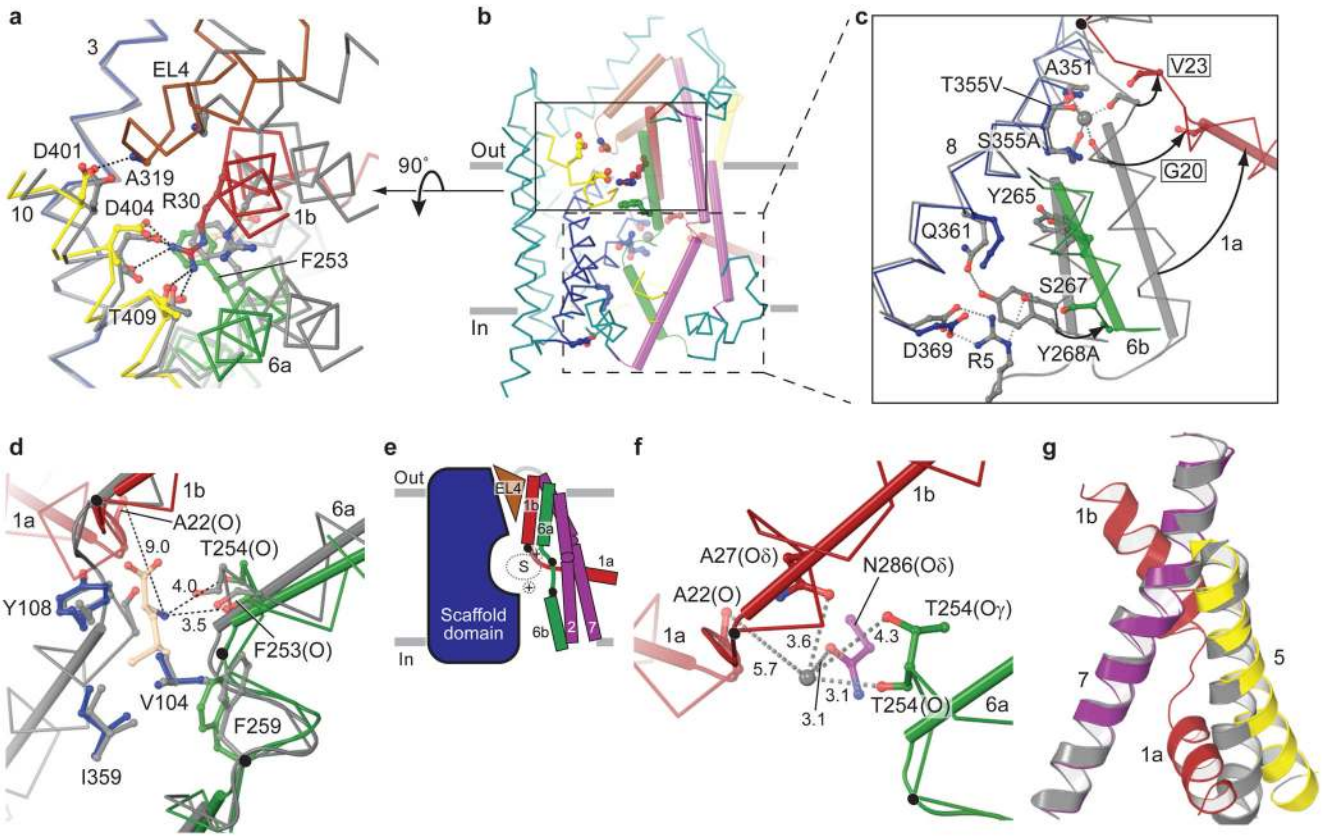

Figure 4. Changes in gate, substrate and ion site interactions and coupling to helix movements

a, Comparison of the extracellular gating interactions in the inward-open and outward-occluded structures. View is from extracellular side. Polar contacts in the inward-open structure are shown as black dashed lines. **b,** Overall view of inward-open structure showing closed extracellular gate (box with solid lines) and open intracellular gate (box with dashed lines). **c,** Comparison of the intracellular gating interactions in the inward-open and outward-occluded structures. Interactions forming the intracellular gate in the outward-occluded state are shown as grey dashed lines. **d,** Changes in the central substrate binding site. In comparing the outward-occluded and inward-open structures, A22, T254, and F253 move away from the binding site. Distances were measured relative to leucine from the outward-occluded structure. **e,** A cartoon representing changes in the core domain relative to scaffold domain and location of hinges relative to position of substrate and ion binding sites is shown, with the pink lines indicating a closed extracellular pathway. **f,** Changes in the Na1 site. Distances of the coordinating residues from sodium ion of the outward-occluded structure are shown. **g,** Superposition of the inward-open and outward-occluded structures using TM7. TM1a of only the inward-open structure is shown for clarity. Coloring scheme as representations are as in Figure 1. Location of TM1 and TM6 hinges are shown as black spheres in **c, d, e, and f**.

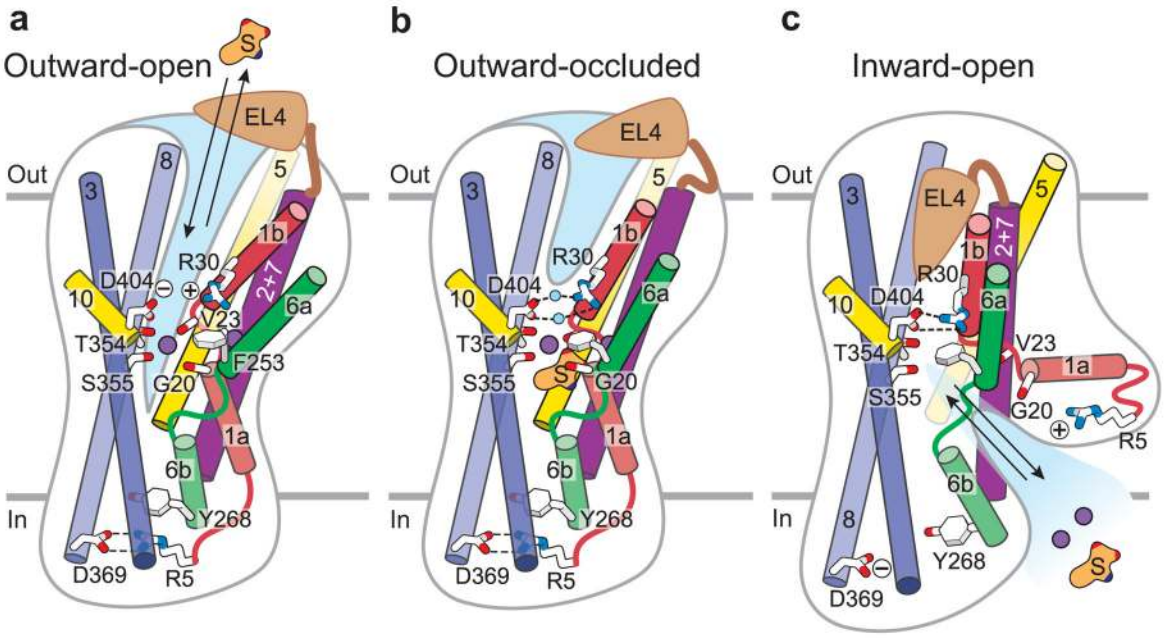

Figure 5. Schematic of transport in LeuT

Shown are structural elements and gating residues instrumental to conformational changes associated with the transition from the outward-open (**a)** to the outward-occluded state (**b**) and the inward-open state (**c**). At present there is no crystal structure for an inward-occluded state and thus no schematic is provided.